

## Controlled Synthesis, Physicochemical and Magnetic Properties of Nano-Crystalline Mn Ferrite System

N. M. Deraz\*, A. Alarifi

Catalytic Chemistry Chair, Chemistry Department, College of Science, King Saud University, P.O. Box 2455, Riyadh 11451, Saudi Arabia

\*E-mail: [nmderaz@yahoo.com](mailto:nmderaz@yahoo.com)

Received: 7 May 2012 / Accepted: 20 May 2012 / Published: 1 June 2012

---

Manganese ferrite nano-particles are synthesised by combustion route by using a mixture of glycine and ammonium nitrate as fuels with corresponding metal nitrates. The nano-sized Mn ferrite characterized by X-ray diffraction (XRD), Scanning electron micrographs (SEM) and Energy dispersive X-ray (EDX) techniques. When the mixture of glycine and ammonium nitrate is used, moderate crystalline  $\text{MnFe}_2\text{O}_4$  is obtained as a single phase with irregular shape. Both the saturation magnetization (80 emu/g) and the remnant magnetization (50 emu/g) were found to be highly depending upon the size and crystallinity of the investigated ferrite. Our results indicate that this method might provide a promising option for synthesizing high-quality nano-sized  $\text{MnFe}_2\text{O}_4$  which has the same saturation magnetization value of bulk Mn ferrite.

---

**Keywords:** XRD; SEM, EDX;  $M_s$ ,  $\text{MnFe}_2\text{O}_4$  nano-particles; magnetic properties

### 1. INTRODUCTION

In recent years, various technological applications are based on nano- ferrite materials due to unique magnetic and electrical properties. It is well known that the physical and chemical properties of the nano-sized magnetic materials are quite different from that of the bulk ones due to their surface effect (large surface-to-volume ratio) and quantum confinement effects (size- dependent properties). Manganese ferrite ( $\text{MnFe}_2\text{O}_4$ ) nano-particles are very important due to their magnetic applications, such as recording media devices, drug delivery, ferrofluid, biosensors and catalysis [1-5].

It is well known that  $\text{MnFe}_2\text{O}_4$  material has inverse spinel structure because 80% of Mn ions occupy tetrahedral site (A-site), which is surrounded by four  $\text{O}^{2-}$  ions, and the left 20% of Mn ions occupy octahedral site (B-site), which is surrounded by six  $\text{O}^{2-}$  ions [6,7]. However, manganese ferrite

belongs to the space group  $Fd3m$ . Many preparation technologies of manganese ferrites such as sol-gel, auto-combustion, thermal decomposition, hydrothermal, ball milling, reverse micelle synthesis, solid-phase reaction, thermally activated solid state reaction and pulsed laser deposition have been developed to prepare the single-domain  $MnFe_2O_4$  nanoparticles [5- 18].

The solid state reaction between iron and manganese oxides was occurred at temperature starting from 900 °C to produce Mn ferrite. The extent of this reaction was increased by increasing the heating temperature in the range of 900-1100 °C [18]. In fact, the minute amounts of  $Mn_2O_3$  and  $Fe_2O_3$  were detected in the final product. It was reported that at elevated temperatures,  $MnFe_2O_4$  is unstable in air and  $Mn^{2+}$  ions on the surface oxidize to form  $Mn^{3+}$  ions resulting in the dissociation of the formed  $MnFe_2O_4$  [19]. So that any preparation method involves calcination step is not suitable for the preparation of manganese ferrite nano-particles. In addition, single-domain manganese ferrite nano-particles have been synthesized with narrow particle size distribution and regular shape via the combustion technique by using glycine [5]. Authors reported that the maximum magnetization and coercivity values of the Mn ferrite were found to be 68.58 emu/g and 62.57 Oe, respectively.

Till now, the detailed study on the structural, morphological and magnetic properties for the  $MnFe_2O_4$  nano-particles synthesized by combustion route using a mixture of glycine and ammonium nitrate has not yet been reported. The present work reports the structural, morphemically and magnetic, properties of manganese ferrite system prepared by new combustion route. The techniques employed were XRD, SEM, EDX and VSM.

## 2. EXPERIMENTAL

### 2.1. Materials

Mn/Fe mixed oxide sample was prepared by mixing calculated proportions of manganese and iron nitrates with a mixture of glycine and ammonium nitrate. The mixed precursors were concentrated in a porcelain crucible on a hot plate at 350 °C for 10 minutes. The crystal water was gradually vaporized during heating and when a crucible temperature was reached, a great deal of foams produced and spark appeared at one corner which spread through the mass, yielding a brown voluminous and fluffy product in the container. In our experiment, the ratio of the  $H_4NNO_3$ :  $H_2NCH_2COOH$ :  $Mn(NO_3)_2 \cdot 4H_2O$  :  $Fe(NO_3)_3 \cdot 9H_2O$  were 1: 4 : 1 : 2, respectively. The chemicals employed in the present work were of analytical grade supplied by Prolabo Company.

### 2.2. Techniques

An X-ray measurement of various mixed solids was carried out using a BRUKER D8 advance diffractometer (Germany). The patterns were run with  $Cu K_\alpha$  radiation at 40 kV and 40 mA with scanning speed in  $2\theta$  of  $2^\circ \text{ min}^{-1}$ .

The crystallite size of Mn-ferrite present in the investigated solids was based on X-ray diffraction line broadening and calculated by using Scherrer equation [20].

$$d = \frac{B\lambda}{\beta \cos \theta} \quad (1)$$

where  $d$  is the average crystallite size of the phase under investigation,  $B$  is the Scherrer constant (0.89),  $\lambda$  is the wave length of X-ray beam used,  $\beta$  is the full-width half maximum (FWHM) of diffraction and  $\theta$  is the Bragg's angle.

Scanning electron micrographs (SEM) were recorded on SEM-JEOL JAX-840A electron microanalyzer (Japan). The samples were dispersed in ethanol and then treated ultrasonically in order to disperse individual particles over a gold grid.

Energy dispersive X-ray (EDX) analysis was carried out on Hitachi S-800 electron microscope with an attached kevox Delta system. The parameters were as follows: accelerating voltage 10, 15 and 20 kV, accumulation time 100s, window width 8  $\mu\text{m}$ . The surface molar composition was determined by the Asa method, Zaf-correction, Gaussian approximation.

The magnetic properties of the investigated solids were measured at room temperature using a vibrating sample magnetometer (VSM; 9600-1 LDJ, USA) in a maximum applied field of 15 kOe. From the obtained hysteresis loops, the saturation magnetization ( $M_s$ ), remanence magnetization ( $M_r$ ) and coercivity ( $H_c$ ) were determined.

### 3. RESULTS

#### 3.1. XRD investigation

The XRD pattern of the as synthesized solid is shown in Fig.1.

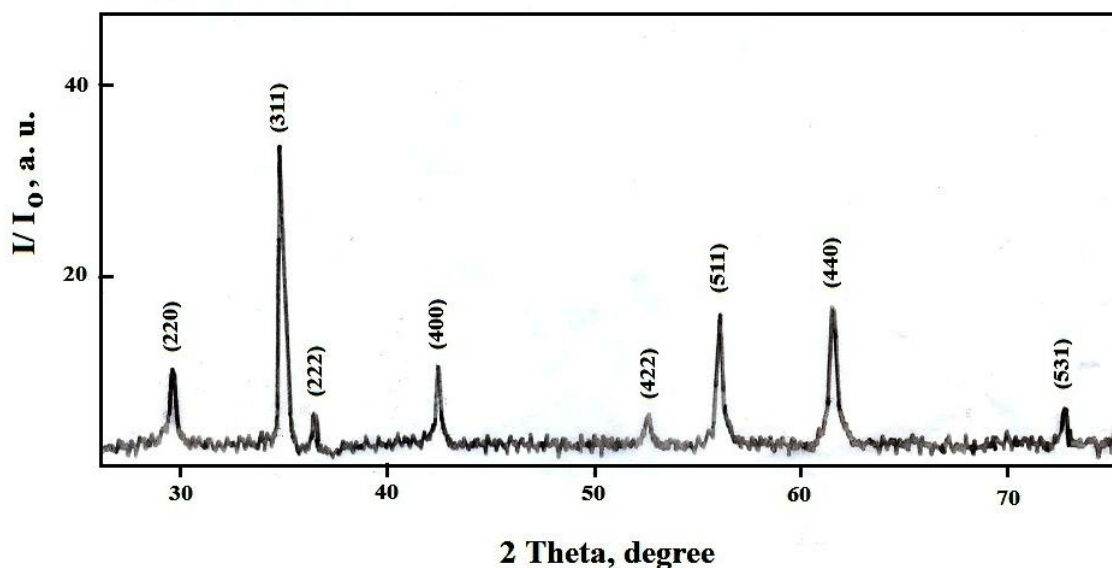
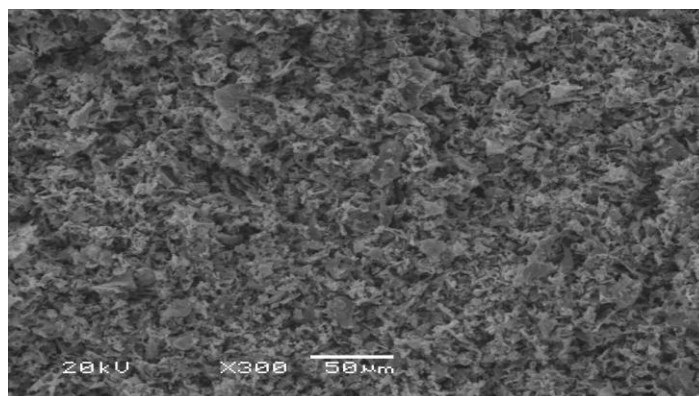
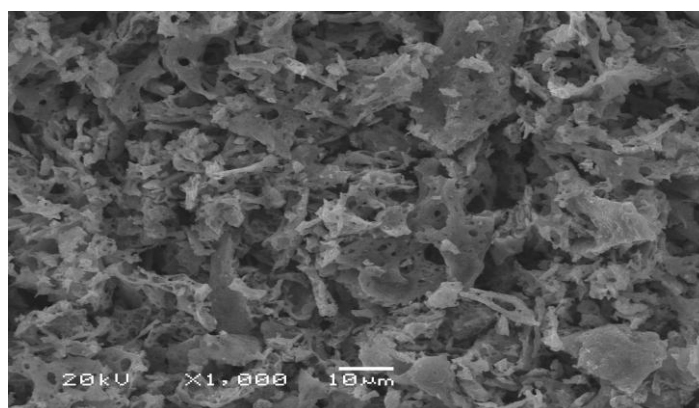


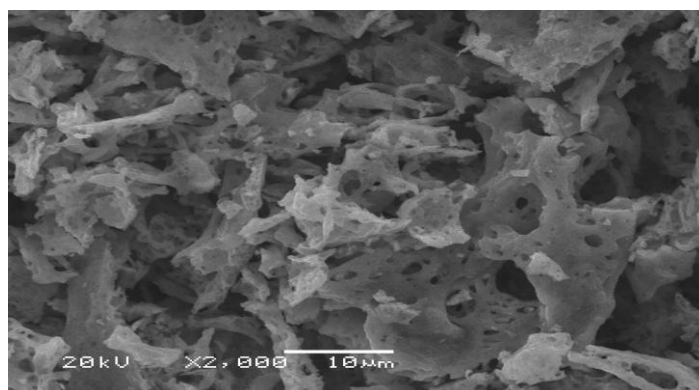
Figure 1. XRD pattern for cubic spinel  $\text{MnFe}_2\text{O}_4$  nano-particles.



a



b



c

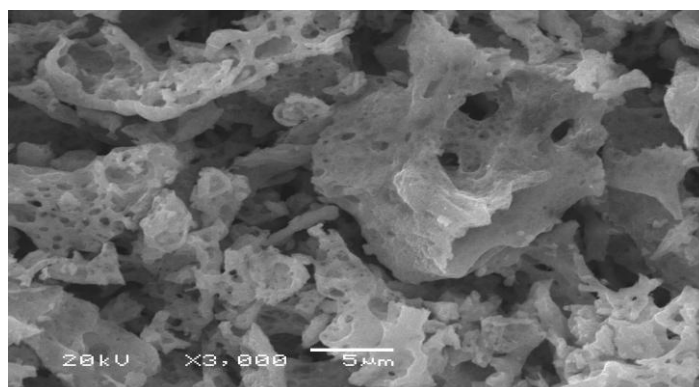


**Figure 2.** SEM images for MnFe<sub>2</sub>O<sub>4</sub> nano-particles with different magnifications.

This figure revealed that the as prepared sample consisted entirely of well nano-crystalline  $\text{MnFe}_2\text{O}_4$  solid. Indeed, the XRD pattern contains eight sharp lines coincide with the standard data of the cubic spinel Mn ferrite (Jacobsite) phase (JCPDS card No. 75-0034). The peaks obtained indexed to the crystal plane of spinel Mn ferrite (220), (311), (222), (400), (422), (511), (440) and (531) respectively. In fact, the XRD pattern does not contain extra peaks for any impurities indicating to formation of Mn ferrite as a single phase. As compared with my previous work, the crystallinity of the manganese ferrite in this work is less than that in the previous work which carried out the glycine as fuel. This indicates the role of ammonium nitrate when it mixed with glycine during the preparation process. Indeed, the crystallite size of the as prepared manganese ferrite was 30 nm.

An X-ray data enable us to calculate the different structural parameters such as the lattice constant ( $a$ ), unit cell volume ( $V$ ), X-ray density ( $D_x$ ), the distance between the magnetic ions ( $L_A$  and  $L_B$ ), ionic radii ( $r_A$ ,  $r_B$ ) and bond lengths (A–O and B–O) on tetrahedral (A) sites and octahedral (B) sites of cubic spinel structure for the produced magnesium ferrite crystallites. The estimated values of  $a$ ,  $L_A$ ,  $L_B$ ,  $r_A$ ,  $r_B$ , A–O and B–O of Mn ferrite are 0.8461, 0.3683, 0.3007, 0.0566, 0.0734, 0.19156 and 0.2084 nm, respectively. Whereas, the value of  $V$  is  $0.6057 \text{ nm}^3$  while the value of  $D_x$  is  $5.0583 \text{ g/cm}^3$ .

### 3.2. SEM measurement

SEM micrographs of as-prepared powders with different magnifications are shown in Fig. 2a-d.

This figure displays the formation of spongy and fragile solid. In addition, the micrographs reveal fracture surfaces of the aggregated powders. In other words, the as synthesized sample consisted of multigrain agglomerations with small discrete crystallites. However, the voids and pores present in the samples are attributed to the release of large amount gases during combustion process. By comparing with my previous work, it is found that the manganese ferrite prepared by using a mixture of glycine and ammonium nitrate displays weak agglomeration.

### 3.3. EDX analysis

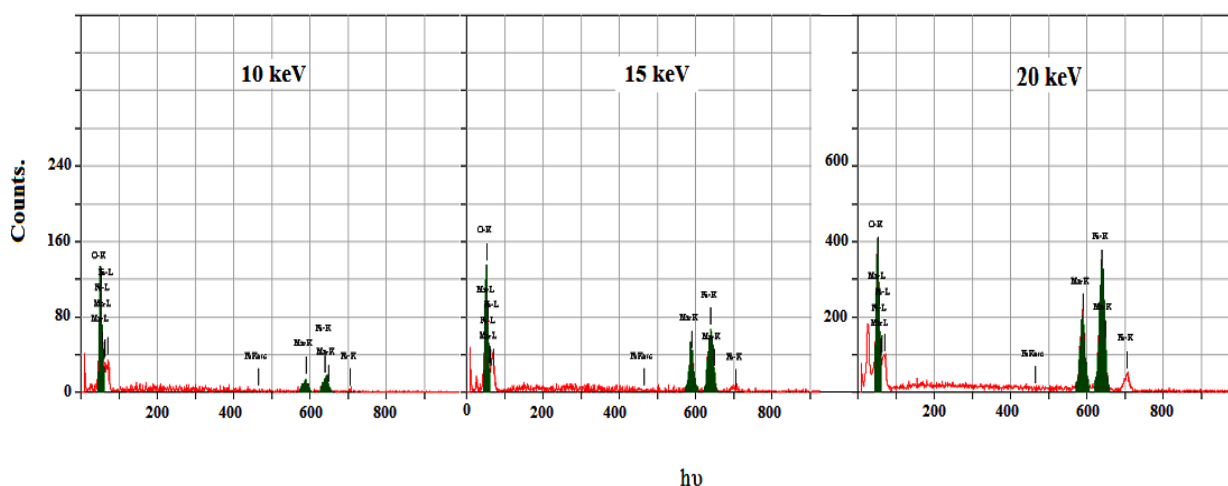


**Figure 3.** EDX pattern of  $\text{MnFe}_2\text{O}_4$  nano-particles with different voltages.

Energy dispersive X-ray (EDX) analysis of the as prepared specimen was carried out at different voltages and various areas on the surface of solid. Figs. 3 and 4 display EDX analysis with different voltages and various areas, respectively.

It is well known that EDX technique supplies the effective atomic concentration of different constituents on top surface layers of the solid investigated. The relative atomic abundance of Mn, Fe and oxygen species present in the uppermost surface and bulk layers of the investigated solid are given in Tables 1 and 2. These tables revealed that the surface concentrations of Mn and Fe species at 10, 15 and 20 keV are very close to those in the bulk of the as synthesized solid. This observation may be reported to the increase in the mobility of Mn and Fe species with subsequent an increase in the formation of Mn ferrite. In addition, the surface concentrations of Mn, Fe and oxygen species at 20 keV on different areas over the surface of specimen studied are much closed to each other. This finding shows the homogeneity of the as prepared solid.

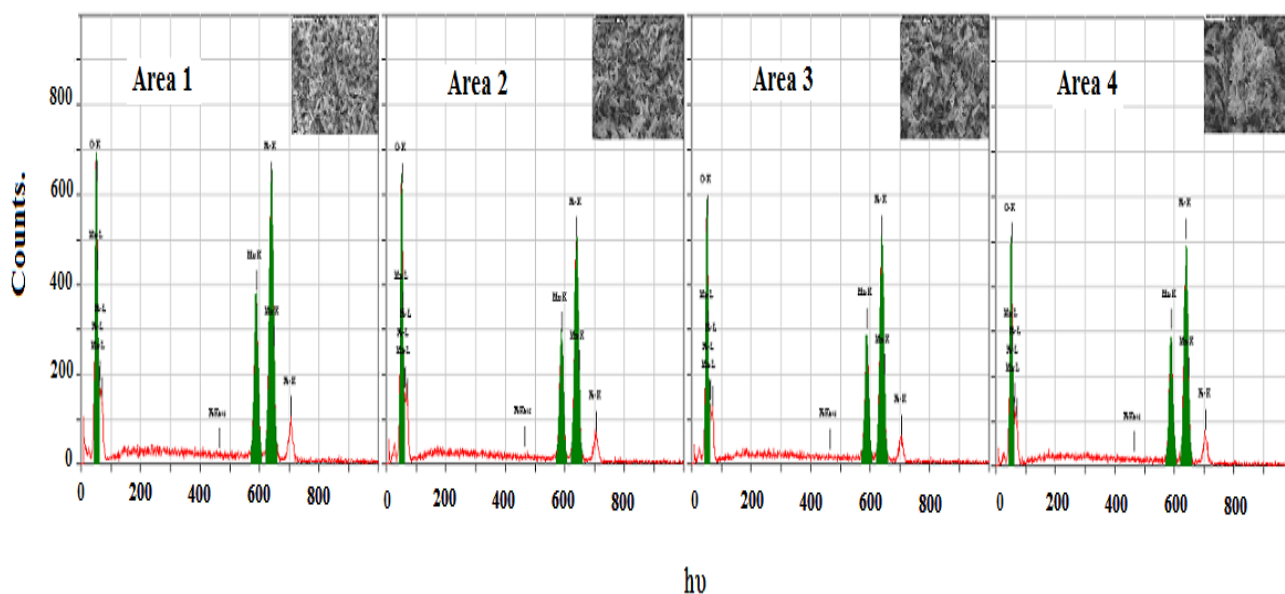


**Figure 4.** EDX pattern of MnFe<sub>2</sub>O<sub>4</sub> nano-particles with different areas.

**Table 1.** The atomic abundance (calculated and found) of elements measured at different voltages over the same area for the as prepared solids.

Elements	Atomic abundance (%)			
	Calculated (Bulk)	Found (Surface)		
		10 keV	15 keV	20 keV
O	27.75	22.36	22.37	22.36
Mn	23.82	24.20	27.41	26.01
Fe	48.43	53.44	50.12	51.63

**Table 2.** The atomic abundance (found) of elements measured at 20 keV and different areas over the as prepared solids.

Elements	Area 1	Area 2	Area 3	Area 4
O	22.36	22.36	22.36	22.36
Mn	25.75	24.81	25.34	25.05
Fe	51.89	52.83	52.30	52.59

### 3.4. Magnetic properties

The magnetic properties of the as-prepared powders were characterized by measuring the magnetic hysteresis loop at room temperature. The saturation magnetization ( $M_S$ ) obtained at room temperature was found to be 80 emu/g and remanent magnetization ( $M_r$ ) was 50 emu/g for the sample studied. The corresponding squareness ratio ( $M_r/M_S$ ) was found to be 0.625. It was found that the as-prepared Mn ferrite particles exhibited a saturation magnetization greater than that of  $MnFe_2O_4$ , prepared by glycine as fuel [5]. In addition the coercivity of the investigated sample was found to 85 Oe. The value of saturation magnetization is very close to the value reported for the bulk  $MnFe_2O_4$  (80 emu/g) [21, 22].

## 4. DISCUSSION

Mn ferrite material can be prepared via solid state reaction between  $Mn_2O_3$  and  $Fe_2O_3$  [18]. The propagation of this reaction is controlled by thermal diffusion of Mn and Fe cations through the ferrite film which covers the surfaces of grains of reacting oxides and acts as energy barrier. The precursor compounds, preparation method and preparation conditions have different effects on solid state reaction between ferric and manganese oxides to produce Mn ferrite. In this study, the combustion route was used for preparation of manganese ferrite. Indeed, the nature of fuel used in this method affect the different properties of the as prepared ferrite. Such properties were particle size, crystallinity, cation distribution, microstructure, homogeneity and magnetic moment...etc. In fact, fuelling of the combustion process achieved by ammonium nitrate produces from combination of nitrate and ammonium ions liberated from decomposition of the reactants [23]. So, addition of ammonium nitrate to the used fuel promotes the combustion process and also reduces the possibility of local partial sintering among the primary particles via dissipation the heat of combustion reaction through the whole mass investigated [24,25].

In addition, the released heat and gases during the combustion process helps in crystallization and formation of  $MnFe_2O_4$  phase with less agglomeration. In other words, the use of ammonium nitrate is promising route for formation of moderate crystalline manganese ferrite nano- particles due to distribution the energy inside the whole reacting particles reducing the aggregation process as shown in SEM micrographs. In addition, XRD measurement showed that Mn ferrite prepared by a mixture of glycine and ammonium nitrate has crystallinity less than that prepared by glycine only [5]

MnFe<sub>2</sub>O<sub>4</sub> particles are formed by the counter-diffusion of Mn<sup>2+</sup> and Fe<sup>3+</sup> through a relatively rigid oxide lattice [5]. During the combustion process, MnO can be prepared by the reduction of any higher oxide [26, 27]. In other words, MnO is prepared by reduction of Mn<sub>2</sub>O<sub>3</sub> producing Mn ferrite via the reaction with Fe<sub>2</sub>O<sub>3</sub> particles. However, Alper [28] reported that the diffusing ions might be Fe<sup>2+</sup> including Fe<sup>3+</sup> on the basis of detecting Fe<sup>2+</sup> in the interface. In addition, following reactions indicate that Fe<sub>2</sub>O<sub>3</sub> decomposes to 2Fe<sup>2+</sup> and oxygen gas at Fe<sub>2</sub>O<sub>3</sub>–spinel interface [29]. Moreover, oxygen moves through the reacted area to be added to the spinel–MgO interface and form spinel by reacting with Fe<sup>2+</sup> and MnO:

At Fe<sub>2</sub>O<sub>3</sub>–spinel interface:



At MnO–spinel interface:



The appearance of any Fe<sup>3+</sup> ions in MnO by diffusion would contribute to the chemically created vacancies depending upon the ionic radii of ferric and magnesium species are 0.080 and 0.065 nm, respectively [30]. In other words, 3Mn<sup>2+</sup> could be replaced by 2Fe<sup>3+</sup> and a vacancy because of electro-neutrality restrictions. Ferric cations which appear in tetrahedral sites with the introduction of trivalent cations into MnO can be considered as an embryonic element or nucleus for formation of inverse spinel in order to satisfy energy stabilization in the structure [31]. On the other hand, Fe<sup>3+</sup> cations have a tendency to be located in tetrahedral sites with making a strong bond with O<sup>2-</sup> ions in terms of electro-negativity differences and reach the lowest state of energy. Mazen and Sabrah reported that the cubic spinel Mn ferrite contains 80% manganese ions (Mn<sup>2+</sup>) in the tetrahedral (A) sites whereas 20% Mn<sup>3+</sup> occupy the octahedral (B) sites [32]. These authors claimed that the trivalent manganese ions are connected by the presence of ferrous ions in the octahedral sites: Mn<sup>2+</sup> + Fe<sup>3+</sup> = Mn<sup>3+</sup> + Fe<sup>2+</sup>. So, the cation distribution for Mn ferrites can be represented by [Mn<sub>0.8</sub><sup>2+</sup> Fe<sub>0.2</sub><sup>3+</sup>]<sub>A</sub> [Mn<sub>0.2</sub><sup>3+</sup> Fe<sub>0.2</sub><sup>2+</sup> Fe<sub>1.6</sub><sup>3+</sup>]<sub>B</sub>O<sub>4</sub> [6, 33]. Using neutron diffraction, Mishra et al. [34] measured the distribution of manganese among tetrahedral and octahedral in the ferrite. These investigators showed that 30% of the octahedral sites are occupied by trivalent manganese ions. Another neutron diffraction experiment performed on the cubic spinel structure of MnFe<sub>2</sub>O<sub>4</sub> nano-particles showed the existence of Mn<sup>2+</sup> and Fe<sup>3+</sup> ions in both the sub-lattices of A and B [35]. So, manganese ferrite is a kind of cubic spinel ferrite material with a partial inverse spinel structure.

In this study, manganese ferrite exhibits super-paramagnetic behavior. This can be attributed to spin canting and surface spin disorder that occurred in these nano-particles [36, 37]. Indeed, the manganese ferrite prepared by a mixture of glycine and ammonium nitrate has saturation magnetization (80 emu/g) greater than that for Mn ferrite synthesized by glycine only (68.58 emu/g) depending upon redistribution of the reacting cations on A and B sites involved in the spinel Mn ferrite by using a mixture of glycine and ammonium nitrate as fuel [5]. In other words, the higher saturation

magnetization of Mn ferrite prepared in this investigation could be attributed migration of some  $\text{Fe}^{3+}$  ions from B site to A site via conversion of some  $\text{Fe}^{2+}$  ions to  $\text{Fe}^{3+}$  ions with subsequent increase in the  $\text{Fe}_A^{3+}\text{-Fe}_B^{3+}$  super-exchange interactions [38]. This conversion brought about an increase in the saturation magnetization and a decrease in the crystallinity of manganese ferrite prepared by a mixture of glycine and ammonium nitrate comparing with that prepared by glycine only due to the contraction in the lattice which depends upon the difference in the ionic radii of both ferric and ferrous ions [5]. Indeed, inter-sublattice super-exchange interactions of the cations on the (A–B) are much stronger than the (A–A) and (B–B) intra-sublattice exchange interactions [39, 40]. However, it has been reported that the spin disorder may occur on the surface of the nano-particles as well as within the cores of the nano-particles due to vacant sub-lattice disorder sites ( $\text{Fe}_A^{3+}$ ) and poor crystal structure [41].

## 5. CONCLUSIONS

Preparation of Mn ferrite via the combustion route using a mixture of glycine and ammonium nitrate as fuel brought about formation of moderate crystalline cubic spinel solid, homogeneously distributed nano-particles with a low grain size. Particle distribution, particle size, homogeneity of solid and cation distribution can be controlled by simply adjusting the ratio of glycine and ammonium nitrate. Manganese ferrite synthesized by the investigated fuel exhibits better magnetic properties depending upon the molar ratio, nature and type of fuel. Higher saturation magnetization (80 emu/g) and coercivity value (50 Oe) are obtained by using a mixture of glycine and ammonium nitrate as fuel. So, the magnetic Mn ferrite materials prepared by the combustion method involved a mixture of glycine and ammonium nitrate as fuel resulted in saturation magnetization greater than those prepared by using glycine only.

## ACKNOWLEDGEMENT

This project was supported by King Saud University, Deanship of Scientific Research, College of Science Research Centre.

## References

1. S. R. Ahmed, S. B. Ogale, G. C. Papaefthymiou, R. Ramesh, P. Kofinas, *Appl. Phys. Lett.* 80(2002)1616
2. I. Brigger, C. Dubernet, P. Couvreur, *Adv. Drug Delivery Rev.* 54 (2002) 631.
3. R. Arulmurugan, G. Vaidyanathan, S. Sendhilnathan, B. Jeyadevan, *J. Magn. Magn. Mater.* 298 (2006) 83.
4. J.B. Haun, T.J. Yoon, H. Lee, R. Weissleder, *Magnetic nanoparticle biosensors*, Wiley Interdiscip. *Rev. Nanomed. Nanobiotechnol.* 2 (2010) 291.
5. N.M. Deraz, S. Shaban, *J. Anal. Appl. Pyrolysis* 86 (2009) 173.
6. M.A. Ahmed, N. Okasha, M.M. El-Sayed, *Ceram. Int.* 33 (2007) 49.
7. Q.M. Wei, Jian-biao Li, Yong-jun Chen, Yong-sheng Han, *Mater. Charact.* 47 (2001) 247.
8. M. H. Mahmoud, H. H. Hamdeh, J. C. Ho, M. J. O'Shea, J. C. Walker, *J. Magn. Magn. Mater.*, 220(2000)139
9. M. Muroi, R. Street, P. G. McCormick, J. Amighian, *Physical Review B.*, 63(2001)184414.
10. C. Li, Z. J. Zhang, *Chem. Mater.*, 13(2001)2092.

11. M. H. Mahmoud, C. M. Williams, J. Cai, I. Siu, J. C. Walker *J. Magn. Magn. Mater.*, 261(2003)314
12. C. Alvani, G. Ennas, A. La Barbera, G. Marongiu, F. Padella, F. Varsano *Int. J. Hydrogen Energy*, 30(2005)1407
13. D. Carta, M.F. Casula, A. Falqui, D. Loche, G. Mountjoy, C. Sangregorio, A. Corrias, *Journal of Physical Chemistry C* 113 (2009) 8606.
14. Y. Liu, Y. Zhang, J.D. Feng, C.F. Li, J. Shi, R. Xiong, *Journal of Experimental Nanoscience* 4 (2009) 159.
15. C. Cannas, A. Musinu, D. Peddis, G. Piccaluga, *Chemistry of Materials* 18 (2006) 3835.
16. C. Cannas, A. Falqui, A. Musinu, D. Peddis, G. Piccaluga, *Journal of Nanoparticle Research* 8 (2006) 255.
17. L.J. Zhao, H.J. Zhang, Y. Xing, S.Y. Song, S.Y. Yu, W.D. Shi, X.M. Guo, J.H. Yang, Y.Q. Lei, F. Cao, *Journal of Solid State Chemistry* 181 (2008) 245.
18. Q. Liu, J.H. Sun, H.R. Long, X.Q. Sun, X.J. Zhong, Z. Xu, *Materials Chemistry and Physics* 108 (2008) 269.
19. N. M. Deraz, *Thermochim. Acta.* 401 (2003) 175.
20. E. D. Macklen, *J. Inorg. Nucl. Chem.* 30 (1968) 2689.
21. B.D. Cullity, *Elements of X-ray Diffraction*, Addison-Wesley Publishing Co. Inc. 1976 (Chapter 14).
22. V.A.M. Brabers, in: K.H.J. Buschow (Ed.), *Handbook of Magnetic Materials*, vol. 8, *Elsevier Science*, New York, 1995, pp. 197–212 pp.
23. A. G. Flores, V. Raposo, J. Iñiguez, L. Torres, S. B. Oseroff, *Physica Status Solidi* 187 (2001)521.
24. P. Priyadharsini, A. Pradeep, G. Chandrasekaran, *J. Magn Magn. Mater.* 321(2009)1898.
25. N. M. Deraz, *Current Applied Physics* 12 (2012) 928.
26. N. M. Deraz, *Int. J. Electrochem. Sci.*, 7 (2012) 4608.
27. Arno H. Reidies "Manganese Compounds" *Ullmann's Encyclopedia of Chemical Technology* 2007; Wiley-VCH, Weinheim.
28. N. N. Greenwood, A. Earnshaw, *Chemistry of the Elements* (2nd ed) (1997), Butterworth-Heinemann, ISBN 0080379419.
29. Alper, *High Temperature Oxides*, Academic Press, New York, 1970.
30. A. Azhari, M. Sharif Sh., F. Golestanifard, A. Saberi, *Mater. Chem. Physics* 124 (2010) 658.
31. O. M. Hemeda, M.A. Amer. S. Aboel-Enein, M. A. Ahmed, *Phys. Stat. Sol.* 156 (1996) 29.
32. S.L. Blank, J.A. Pask, *J. Am. Ceram. Soc.* 52 (1969) 669.
33. S. A. Mazen, B. A. Sabrah, *Thermochim. Acta* 105(1986)1.
34. Q.M. Wei, Jian-biao Li, Yong-jun Chen, Yong-sheng Han, *Mater. Charact.* 47 (2001) 247.
35. S. Mishra, T.K. Kundu, K.C. Barick, D. Bahadur, D. Chakravorty, *J. Magn. Magn. Mater.* 307 (2006) 222.
36. C. Liu, B. Zou, A. J. Rondinone, Z. J. Zhang, *J. Phys. Chem. B* 104(2000)1141.
37. Z. Gu, X. Xiang, G. Fan, F. Li, *J. Phys. Chem. C* 112 (2008) 18459.
38. L. Ai, J. Jiang, *Curr. Appl. Phys.* 10 (2010) 284.
39. L. Jianjun, Y. Hongming, L. Guodong, L. Yanju, L. Jinsong, *J. Magn. Magn. Mater.* 322(2010)3396.
40. M. Atif, S.K. Hasanain, M. Nadeem, *Solid State Commun.* 138 (2006) 416.
41. S. Ammar, N. Jouini, F. Fiévet, Z. Beji, L. Smiri, P. Moliné, M. Danot, J. M. Grenéche, *J. Phys.:Condens. Matter* 18(2006) 9055.
42. M. P. Morales, S. Veintemillas-Verdaguer, M. I. Montero, C. J. Serna, A. Roig, L. Casas, B. Martínez, F. Sandiumenge, *Chem. Mater.* 11(1999)3058.